Electronic Supplementary Material (ESI) for Dalton Transactions.

## Supplementary Information

# Dual stimuli-responsive phosphorescence of a Pb(II) coordination polymer to acidic vapors and thermal treatment

*Sujitra Tunsrichon,* [a] *Kittipong Chainok,* [b] *Vinich Promarak,* [c] *Suangsiri Arunlimsawat,* [c] *Sujittra Youngme* [a] *and Jaursup Boonmak* [a*]

[a] Materials Chemistry Research Center, Department of Chemistry, Faculty of Science, Khon Kaen University, Khon Kaen 40002, Thailand.

[b] Thammasat University Research Unit in Multifunctional Crystalline Materials and Applications (TU-MCMA), Faculty of Science and Technology, Thammasat University, Pathum Thani 12121, Thailand.

[c] School of Molecular Science & Engineering, Vidyasirimedhi Institute of Science and Technology (VISTEC), Wangchan, Rayong 21210, Thailand.

*E-mail: Jaursup@kku.ac.th

## EXPERIMENTAL SECTION

**Materials and Characterization Methods.** All chemical solvents and reagents were purchased directly from the commercial source and used without any purification. Powder X-ray diffraction (PXRD) patterns in 2θ range from 5 to 50° were recorded at a speed of 0.5 s/step by using a Bruker D8 Advance diffractometer with Cu-Kα radiation ($\lambda = 1.5406$ Å). Elemental analyses (C, N, and H) were conducted on a HERMO FLASH 2000 CHNS/O analyzer. The attenuated total reflectance-Fourier transform infrared (ATR-FT-IR) spectra were obtained on a Bruker Tensor 27 FT-IR spectrophotometer using a standard Pike ATR sampling accessory in the range 4000 to 600 $cm^{-1}$. Thermogravimetric analysis (TGA) was performed in the temperature range of 35−800 °C using a Hitachi STA7200 thermal analyzer in nitrogen atmosphere with a heating rate of 10 °C/min. Energy dispersive X-ray spectroscopy (EDS), FEI Helios Nanolab G3 CX, was carried out for the elemental mapping. Luminescent lifetime decay at room temperature was performed on an Edinburgh Instruments FLS980 spectrometer. The absolute photoluminescence quantum yields ($\Phi_{PL}$) were measured using an Edinburgh Instruments FLS980 spectrometer integrated with a calibrated integrating sphere. Solid-state luminescent spectra were recorded at room temperature using a Shimadzu RF-6000 spectrofluorophotometer equipped with a continuous Xe lamp.

**Synthesis of $[Pb(pzt)_2(H_2O)]_n$ (1).** The aqueous solution (1 mL) of $Pb(NO_3)_2$ (0.1 mmol, 33.1 mg) was mixed with DMF solution (1 mL) of Hpzt (0.1 mmol, 17.8 mg) in a 10 mL glass vial. Then 2 mL of MeCN solvent was added. The vial was capped and allowed to stand undisturbed at room temperature. After a day, yellow polycrystals of **1** were produced with a yield of 40% (23.3 mg), based on Hpzt ligand. Anal. Calcd for $PbC_{14}H_{10}N_6O_3S_2$ (581.60 g/mol) C, 28.91; H, 1.73; N, 14.45%. Found C, 29.42; H, 1.39; N, 14.53%. ATR-FT-IR ($cm^{-1}$): 2769-3350 (br), 1587 (w), 1155 (m), 1077 (m), 1020 (s), 950 (w), 690 (s).

The high-quality single crystals of **1** were synthesized by a solvothermal method. The mixed solution of reactants was sealed in a glass Pyrex tube (20 mL) and kept in an oven at 90 °C for 24 h. The rod-like yellow single crystals of **1** were manually separated from other impurity crystals for the structural determination by single-crystal X-ray diffraction.

**Acidochromic Luminescent Test.** A saturated acidic vapor was produced from evaporation of acidic solution (3 mL) in a sealed vial (15 mL) at room temperature. The detail of concentration of the commercial acidic solutions used in this work was presented in Table S4. A small tube (1 mL) containing the powder of **1** (10 mg) was exposed to the acidic vapor in the sealed vial (15 mL) at room temperature. The exposed powder was removed for characterizations and solid-state luminescent studies upon excitation at 389 nm.

**Crystal Structure Determination.** Single-crystal X-ray diffraction (SC-XRD) data were collected on a Bruker D8 QUEST CMOS PHOTON II using a graphite-monochromated Mo Kα ($\lambda$ = 0.71073 Å) radiation at T = 296(2) K. The total number of runs and images was based on the strategy calculated from APEX3 program and unit cell indexing was refined using SAINT.[1] Data integration was conducted using SAINT.[2] The SADABS program was used for absorption correction.[3] The crystal structure was solved by SHELXTL program through intrinsic phasing which uses a full-matrix least-squares on $F^2$ with anisotropic thermal parameters for refinement of all non-hydrogen atoms.[4, 5] Hydrogen atoms were located at geometrically calculated positions and isotropically refined in a riding model. The molecular structures of **1** were drawn using the Diamond 4 program. The crystallographic data, and the selected bond distances and angles of **1** are presented in Tables S1 and S2.

**Table S1.** Crystallographic data of **1**.

| | **1** |
|---|---|
| formula | $PbC_{14}H_{10}N_6O_3S_2$ |
| molecular weight | 581.60 |
| T (K) | 296(2) |
| crystal system | monoclinic |
| space group | $P2_1/n$ |
| $a$ (Å) | 11.2475(2) |
| $b$ (Å) | 7.56440(10) |
| $c$ (Å) | 20.2712(4) |
| α (°) | 90 |
| β (°) | 101.5170(10) |
| γ (°) | 90 |
| $V$ (Å$^3$) | 1689.96(5) |
| $Z$ | 4 |
| $\rho_{\text{cald}}$ (g cm$^{-3}$) | 2.286 |
| $\mu$ (Mo Kα) (mm$^{-1}$) | 10.260 |
| data collected | 53751 |
| unique data ($R_{\text{int}}$) | 4748 (0.0382) |
| $R_1{}^a/wR_2{}^b$ [$I > 2(I\sigma)$] | 0.0224/0.0518 |
| $R_1{}^a/wR_2{}^b$ [all data] | 0.0290/0.0547 |
| GOF | 1.089 |
| Maximum/minimum electron density (e Å$^{-3}$) | 0.83/-1.09 |

$^aR_1 = \Sigma||F_o| - |F_c||/\Sigma|F_o|$. $^bwR_2 = \{\Sigma[w(|F_o| - |F_c|)]^2/\Sigma[w(|F_o|^2]\}^{1/2}$.

**Table S2.** Selected bond distances (Å) and angles (°) for **1**.

| | |
|---|---|
| Pb1−O3 | 2.495(2) |
| Pb1−N3$^{i}$ | 2.641(3) |
| Pb1−N1 | 2.675(2) |
| Pb1−S2 | 2.9652(8) |
| Pb1−S1$^{ii}$ | 3.0157(9) |
| C1−S1$^{ii}$ | 1.706(3) |
| C8−S2 | 1.710(3) |
| O3−Pb1−N3$^{i}$ | 73.64(7) |
| O3−Pb1−N1 | 150.55(7) |
| N3$^{i}$−Pb1−N1 | 76.95(8) |
| O3−Pb1−S2 | 87.89(5) |
| N3$^{i}$−Pb1−S2 | 86.49(6) |
| N1−Pb1−S2 | 88.89(6) |
| O3−Pb1−S1$^{ii}$ | 89.31(6) |
| N3$^{i}$−Pb1−S1$^{ii}$ | 96.71(6) |
| N1−Pb1−S1$^{ii}$ | 95.58(6) |
| S2−Pb1−S1$^{ii}$ | 174.99(2) |

Symmetry codes for **1**: (i) 0.5-x, 0.5+y, 0.5-z; (ii) 1-x, 1-y, 1-z.

**Table S3.** Hydrogen bond lengths (Å) and angles (°) for **1**.

| **D−H···A** | **d(D−H)/Å** | **d(H···A)/Å** | **d(D···A)/Å** | **<(DHA)/°** |
|---|---|---|---|---|
| O(3)−H(3A)···N(6) (Intra) | 0.82 | 2.55 | 3.344(4) | 164 |
| O(3)−H(3B)···N(4) (Intra) | 0.85 | 1.87 | 2.727(3) | 176 |
| C(4)−H(4)···N(5) | 0.93 | 2.59 | 3.400(4) | 145 |
| C(12)−H(12)···O(3) | 0.93 | 1.84 | 2.747(4) | 163 |

**Table S4.** The concentration and the pKa of the commercial acid solutions used in acidochromic luminescent test.

| **Pure acidic solution** | **Concentration (% v/v)** | **pKa** |
|---|---|---|
| Hydrochloric acid (HCl) | 37 | -7 |
| Formic acid (HCOOH) | 99 | 3.75 |
| Sulfuric acid ($H_2SO_4$) | 96 | -2 |
| Perchloric acid ($HClO_4$) | 72 | -10 |
| Acetic acid ($CH_3COOH$) | 99.8 | 4.75 |
| Propionic acid ($CH_3CH_2COOH$) | 98 | 4.87 |
| Nitric acid ($HNO_3$) [a] | 65 | -1.3 |

[a] For $HNO_3$ vapor, the powder of **1** was dissolved, so the $HNO_3$-exposed product could not be characterized.

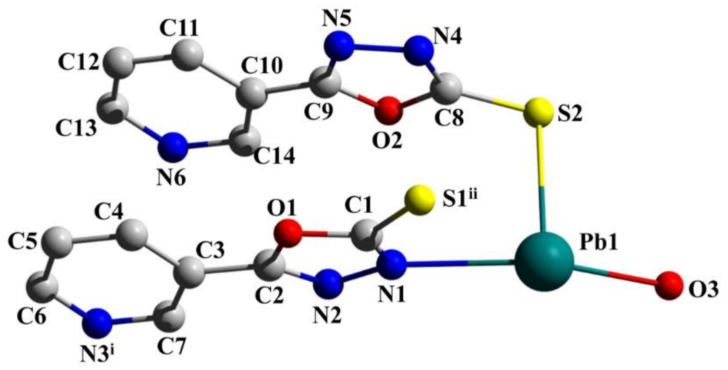

**Fig. S1** The asymmetric unit of **1**. All hydrogen atoms are omitted for clarity. Symmetry codes: (i) 0.5 - x, 0.5 + y, 0.5 - z; (ii) 1 - x, 1 - y, 1 - z.

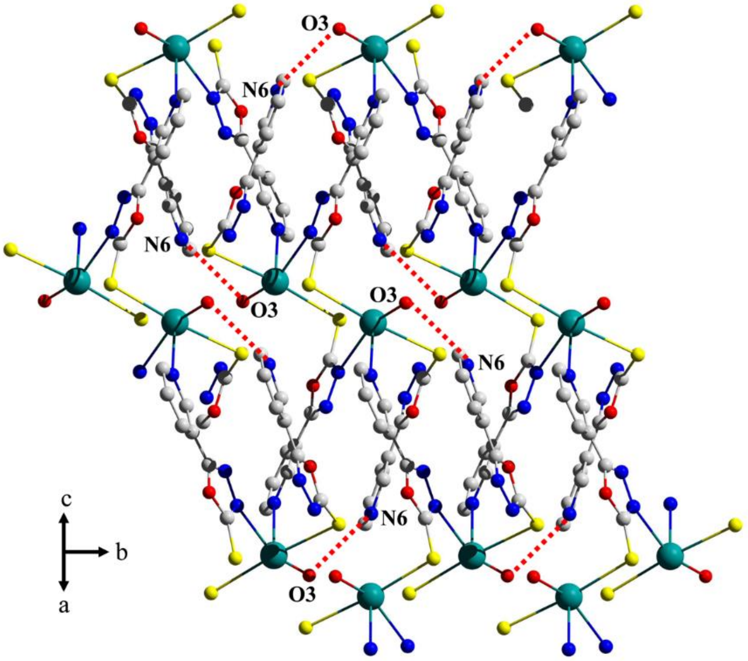

**Fig. S2** A single 2D layer of **1** stabilized by intramolecular hydrogen bonds between an uncoordinated pyridine N atom of the terminal pzt and the aqua ligand (O3H3A···N6 = 3.344(4) Å) (red dashed lines).

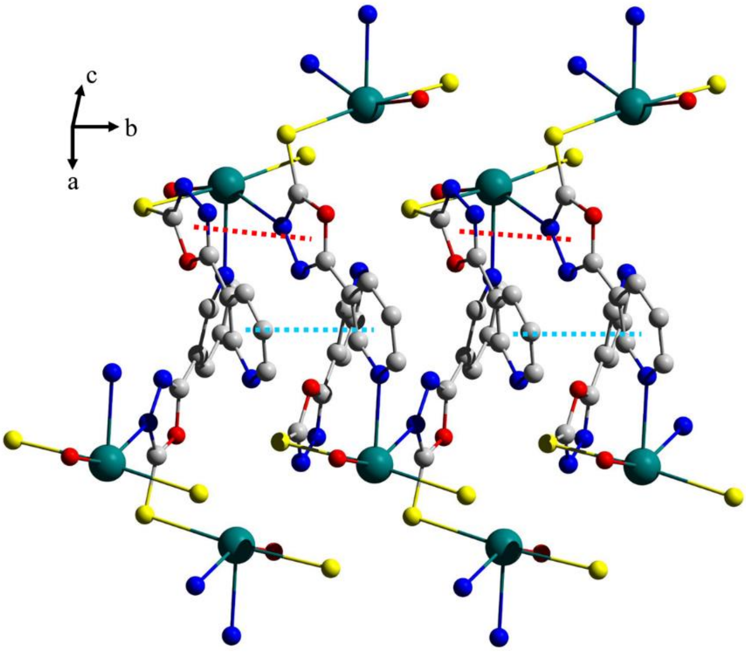

**Fig. S3** A single 2D layer of **1** stabilized by two different π−π interactions including the face-to-face configurations between two opposite pyridine rings ($Cg_{py}\cdots Cg_{py}$ = 3.510(2) Å, blue dashed lines) and two opposite oxadiazole rings ($Cg_{oxa}\cdots Cg_{oxa}$ = 3.739(2) Å, red dashed lines).

**Characterization and Thermal Stability of 1.** The FT-IR spectrum of Hpzt ligand shows peaks of ν(C=N), ν(N−N), $\nu_{as}$(C−O−C), $\nu_{s}$(C−O−C), ν(C−S), and ν(pyridine) at 1618, 1191, 1154, 1070, 901 and 700 cm$^{-1}$, respectively (Fig. S5). These peaks in **1** are shifted to a lower frequency, indicating the formation of coordination bonds between the Pb(II) center and pzt. A broad peak of ν(S−H) at around 2700-2310 cm$^{-1}$ is not observed in **1** because of the deprotonation of Hpzt during the crystallization process. The negative shift of ν(C−S) in Hpzt to 815 cm$^{-1}$ after coordinating assembly, suggesting that the pzt ligand in **1** adopts thiolate form (Fig. S4 and S5). Also, the large shift is probably due to coordination and intramolecular tetrel Pb···S bonds in **1** (Fig. 1b). These results are well agreement with the crystal structure of **1**. The occurrence of a broad peak around 2670-3350 cm$^{-1}$ also supports the coordinated water molecule. Thermal stability of **1** was investigated by TGA in the temperature range of 35−800 °C under an $N_2$ atmosphere (Fig. S6). **1** is thermally sable up to 135 °C, then a single step of weight loss (obsd 3.17%, calcd 3.09%) appears until 175 °C, corresponding to the loss of one coordinated water molecule. From that point on, the structure maintains its thermal stability until 283 °C before continuous decomposition to the unidentified residue. The crystalline phase purity of **1** obtained from the synthesis at room temperature, was confirmed by PXRD results. A good match of diffraction patterns between the as-synthesized **1** and the simulated data from SC-XRD indicates high phase purity of crystal **1** (Fig. S7).

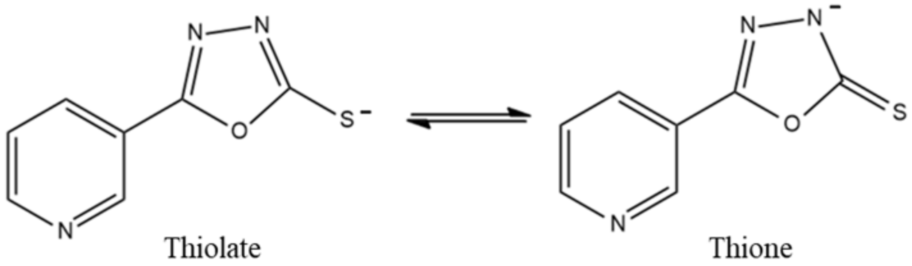

**Fig. S4** Thiolate and thione conformations of pzt ligand.

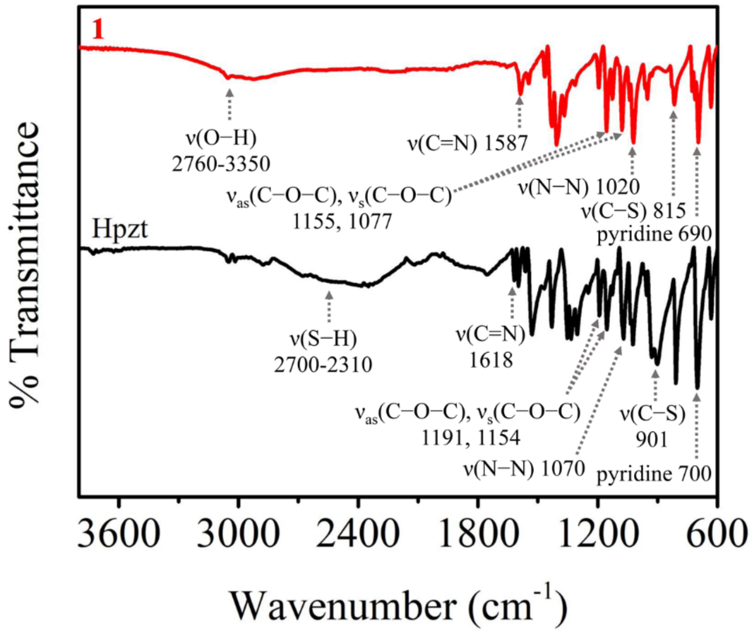

**Fig. S5** FT-IR spectra of **1** and free Hpzt ligand.

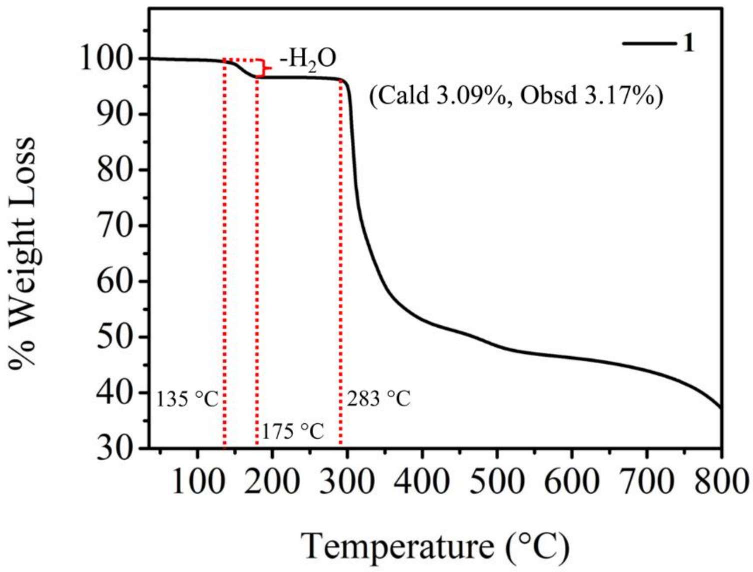

**Fig. S6** TG curve of **1** recorded in $N_2$ atmosphere.

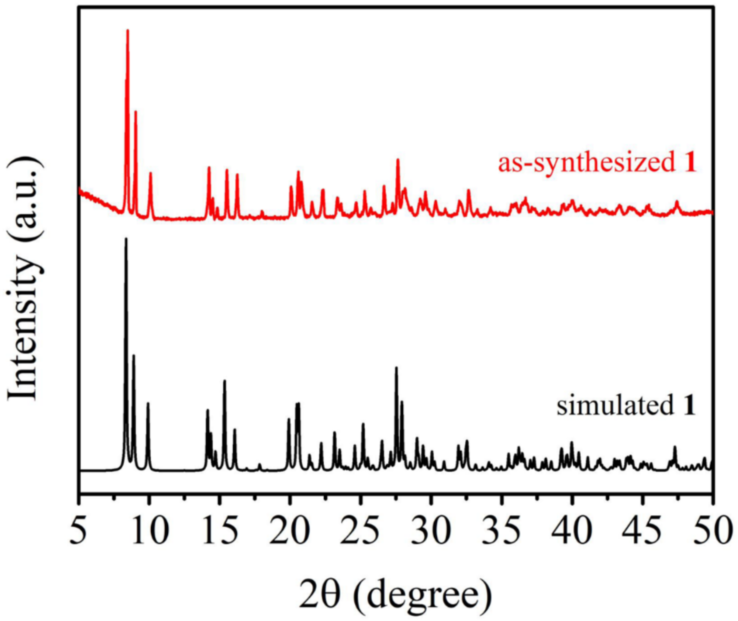

**Fig. S7** PXRD pattern of as-synthesized **1** compared with the simulated pattern.

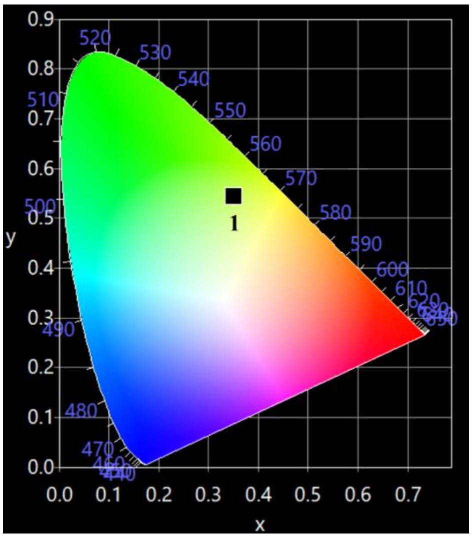

**Fig. S8** The corresponding CIE chromaticity coordinates (x,y) for **1** (0.3508, 0.5417).

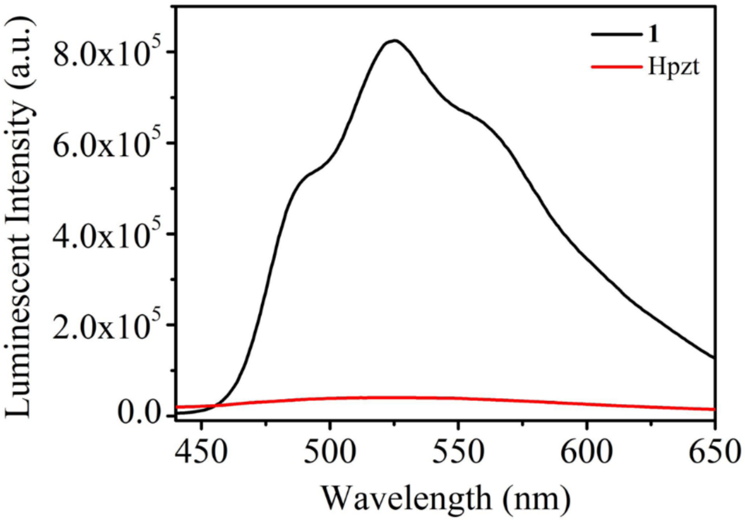

**Fig. S9** Solid-state PL spectrum of **1** compared with the free Hpzt ligand.

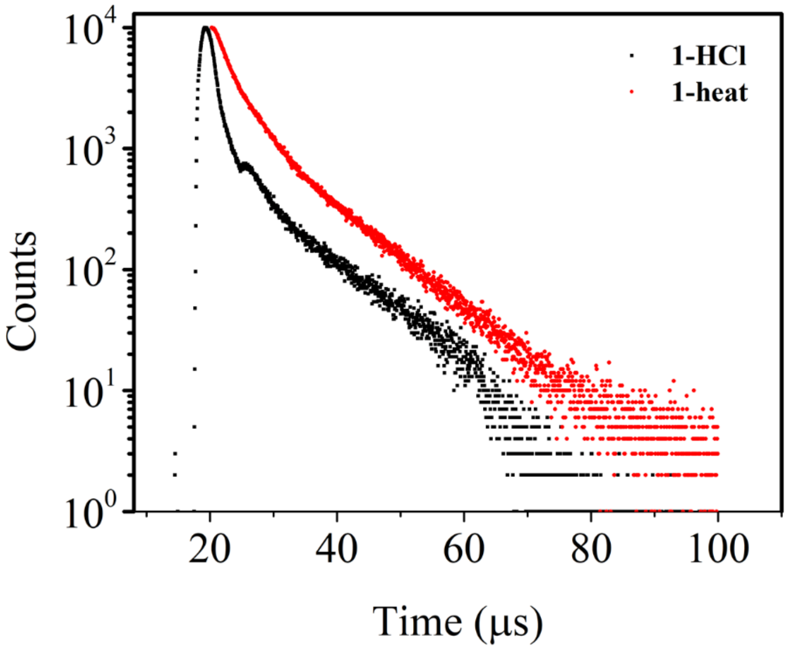

**Fig. S10** Time-resolved phosphorescence decay curves of **1-HCl** ($\lambda_{ex}$ = 389 nm and $\lambda_{em}$ = 449 nm) and **1-heat** ($\lambda_{ex}$ = 414 nm and $\lambda_{em}$ = 546 nm) measured in solid phases at room temperature.

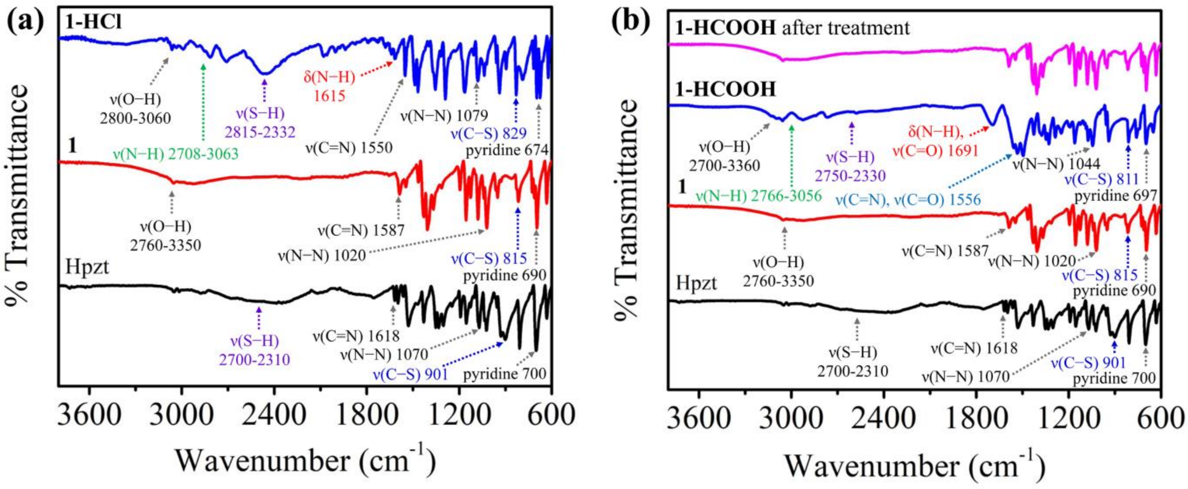

**Fig. S11** FT-IR spectra of (a) **1-HCl**, and (b) **1-HCOOH** and **1-HCOOH** after treatment compared with the original **1** and the free Hpzt ligand.

**Table S5.** Photoluminescence quantum yield and lifetime of the reported Pb(II)-based coordination compounds in solid state recorded at room temperature.

| **Compounds** | **$\lambda_{em}$ (nm)** | **$\Phi_{PL}$** | **Lifetime ($\tau$)** | **Ref.** |
|---|---|---|---|---|
| **$[Pb(pzt)_2(H_2O)]_n$ (1)** | **526** | **21.62%** | **25.46 µs** | **This work** |
| $(PiperA)_2PbBr_4$ | 500 | 7.1% | 3.2 ms | 6 |
| $(TOBA)_2PbBr_4$ | 580 | 0.7% | 1.2 ms | 6 |
| $[Pb_2O(C_6H_4NO_2)_2]_n$ | 510 | 59.4% | 9.86 ms | 7 |
| $[Pb(phen)Cl_2]$ | 576<br>646<br>718 | 9.67% | 0.61 ms<br>4.61 ms<br>1.32 ms | 8 |
| $[Pb_2(HBTC)_2(DMF)]$ | 550 | 1.2% | 0.73 ms | 9 |
| $[Pb(HPTC)]$ | 560 | 4.7% | 1.52 ms | 9 |
| $[Pb(2\text{-}anc)_2]_n$ | 548 | 2.2% | $\tau_1 = 0.12$ ms, $\tau_2 = 1.14$ ms | 10 |
| $Bmpip_2PbBr_4$ | 470 | 24% | $\tau_1 = 230$ ps, $\tau_2 = 66$ ns | 11 |
| $[Pb(3\text{-}qlc)_2(H_2O)_2]_n$ | 430 | 3.5% | $\tau = 0.78$ ns | 10 |
| $[PbCl_2(bp_4mo)]$ | 600 | 6% | 250 µs | 12 |
| $[PbBr_2(bp_4mo)]$ | 600 | 22% | 250 µs | 12 |
| $[PbI_2(bp_4mo)]$ | 600 | 27% | 40 µs | 12 |
| $[Pb_5(L_1)_6(N_3)_2(OH)_2]_n$ | 632 | - | 5.5 µs | 13 |
| $[Pb(L_2)(N_3)]_n$ | 602 | - | 7.1 µs | 13 |
| $[Pb(L^1)_2]_n$ | 539 | 1.0% | 1550 µs | 14 |
| $[Pb(L^2)_2]_n$ | 620 | 1.5% | 2570 µs | 14 |
| $[Pb(L^3)(NO_3)(H_2O)_2]_n$ | 570 | 1.8% | 252.5 µs | 14 |
| $[Pb(L^3)(Br)(H_2O)]_n$ | 615 | 2.0% | 351.0 µs | 14 |
| $[Pb(L^3)(Cl)(H_2O)]_n$ | 645 | 16.5% | 498.7 µs | 14 |
| $[Pb(L^4)(H_2O)_2]$ | 593 | 2.0% | 347.5 µs | 14 |
| $[Pb(NO_3)_2(bp_4mo)]$ | 600 | 34% | $\tau_1 = 1.5$ µs, $\tau_2 = 700$ µs | 12 |
| *trans*-$[Pb(DMTU\text{-}S)_4Cl_2]$ | 549 | 91% | $\tau_1 = 0.02$ ms, $\tau_2 = 3.8$ ms | 15 |
| $[Pb(FDA)(H_2O)]$ | 491 | 14.9% | 0.62 ms | 16 |
| $[NH_3(CH_3)NH_2(CH_3)_2][Pb_4(FDA)_5]$ | 570 | 15.7% | 1.69 ms | 16 |
| $[Pb_4(\mu_2\text{-}OH)(\mu_3\text{-}OH)(\mu_4\text{-}O)(3\text{-}qlc)_4]_n$ | 589 | 3.3% | 1.52 ms | 17 |
| $[Pb(TDC)]_n$ | 612 | 6.7% | 1.78 ms | 18 |
| $[Pb_2(EBTC)(DMSO)_3]$ | 560 | 1.5% | 4.17 ms | 19 |
| $[Pb_4(OH)_4(BDT)_2](H2O)_2$ | 552 | - | $\tau_1 = 0.247$ ms, $\tau_2 = 0.0279$ ms | 20 |
| $[Pb_4(OH)_4(BDT)](BDT)(H_2O)_2$ | 552 | - | $\tau_1 = 0.24$ ms, $\tau_2 = 0.0513$ ms | 20 |
| $[Pb(TFIPA)(2,2'\text{-}bpy)]_n$ | 384 | 1.23% | 1.25 ns | 21 |
| $[Pb(TFIPA)(1,10\text{-}phen)]_n$ | 384 | 1.36% | 1.32 ns | 21 |
| $[Pb(TFIPA)(4,40\text{-}bpy)_{0.5}(H_2O)]_n$ | 384 | 1.79% | $\tau_1 = 1.47$ ns, $\tau_2 = 1.68$ µs | 21 |
| $[Pb(TFIPA)(4,40\text{-}bpy)_{0.5}(H_2O)]_n$ | 384 | 1.29% | 1.28 ns | 21 |
| $\{[Pb_4(OH)_2(SIP)_2(H_2O)](H_2O)_5\}_n$ | 436 | - | 2.43 ns | 22 |
| $\{[Pb_4(OH)_2(SIP)_2(H_2O)](H_2O)_5\}_n$ | 603 | - | 3.47 µs | 22 |
| $[Pb_2(L)_2]_n$ | 566 | - | $\tau_1 = 0.597$ ns, $\tau_2 = 2.294$ ns | 23 |
| $[Pb_3(L)_3]_n$ | 581 | - | $\tau_1 = 0.780$ ns, $\tau_2 = 3.363$ ns | 23 |
| $[Pb(L)](H_2O)$ | 505 | - | $\tau_1 = 0.540$ ns, $\tau_2 = 3.771$ ns | 23 |
| $[Pb(Mq)_2]_2(H_2O)_3$ | 480 | - | 0.04 ns | 24 |
| $[Pb_4(Mq)_6](ClO_4)_2$ | 475 | - | 0.08 ns | 24 |
| $[Pb(triBZ\text{-}NTB)_2](NO_3)_2(H_2O)_2$ | 450 | - | 0.80 ns | 24 |
| $\{[PbZn(HtriCB\text{-}NTB)(DMF)Cl_2]\}_n$ | 443 | - | 0.90 ns | 24 |
| Pb-SMOF-Cl | 534<br>575<br>630 | - | 15.96 µs<br>16.06 µs<br>17.08 µs | 25 |
| $[Pb(bib)(NO_3)_2]_n$ | 447 | - | 4.0 ns | 26 |

$\lambda_{em}$ = maximum emission wavelength, $\Phi_{PL}$ = photoluminescence quantum yield

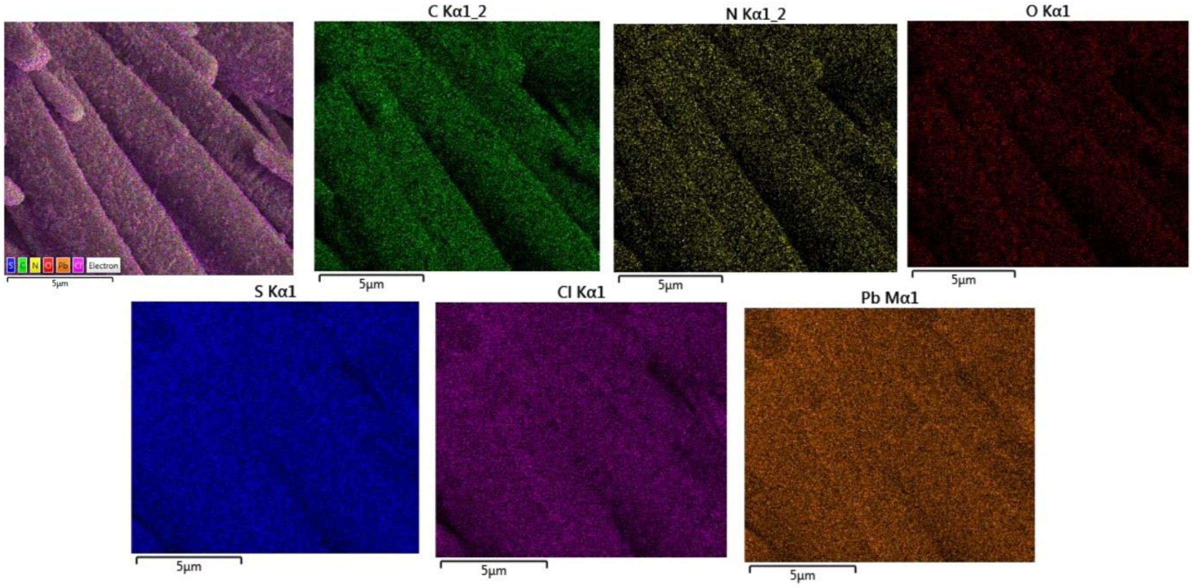

**Fig. S12** Elemental distribution maps of **1-HCl**.

**Table S6.** CHN analysis results.

| Compounds | Formulae | Cald. CHN (%) | Obsd. CHN (%) |
|---|---|---|---|
| **1-HCl** | $PbCl_4(H_2pzt)_2(H_2O)$ | C, 23.12; H, 1.94; N, 11.55 | C, 22.94; H, 1.53; N, 11.31 |
| **1-HCOOH** | $Pb(pzt)(H_2pzt)(HCOO)_2(HCOOH)_3(H_2O)$ | C, 28.11; H, 2.48; N, 10.35 | C, 27.97; H, 1.91; N, 10.59 |
| **1-heat** | $[Pb(pzt)_2]_n$ | C, 29.84; H, 1.43; N, 14.91 | C, 29.81; H, 1.24; N, 14.73 |

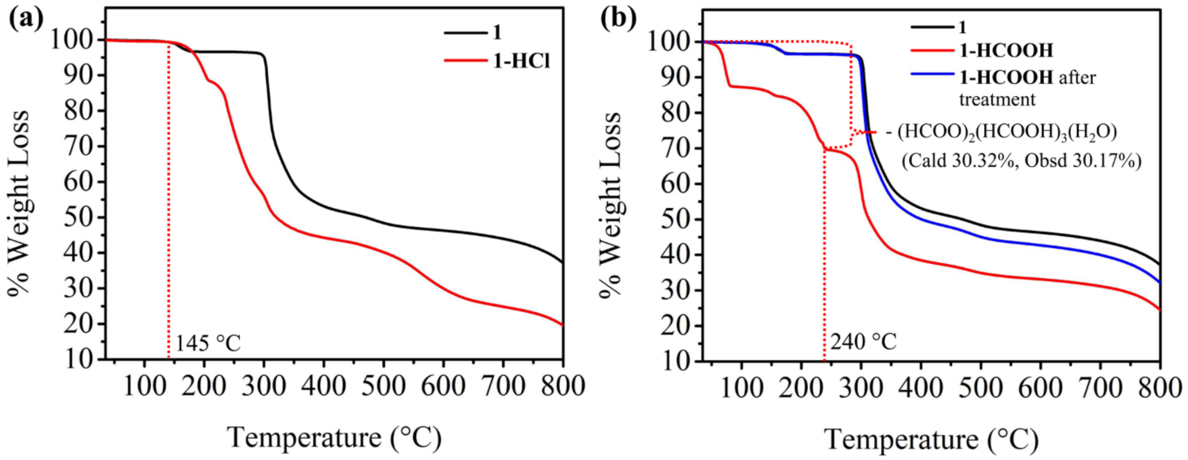

**Fig. S13** TG curves of **1-HCl** (a) and **1-HCOOH** before and after treatment (b) recorded in $N_2$ atmosphere.

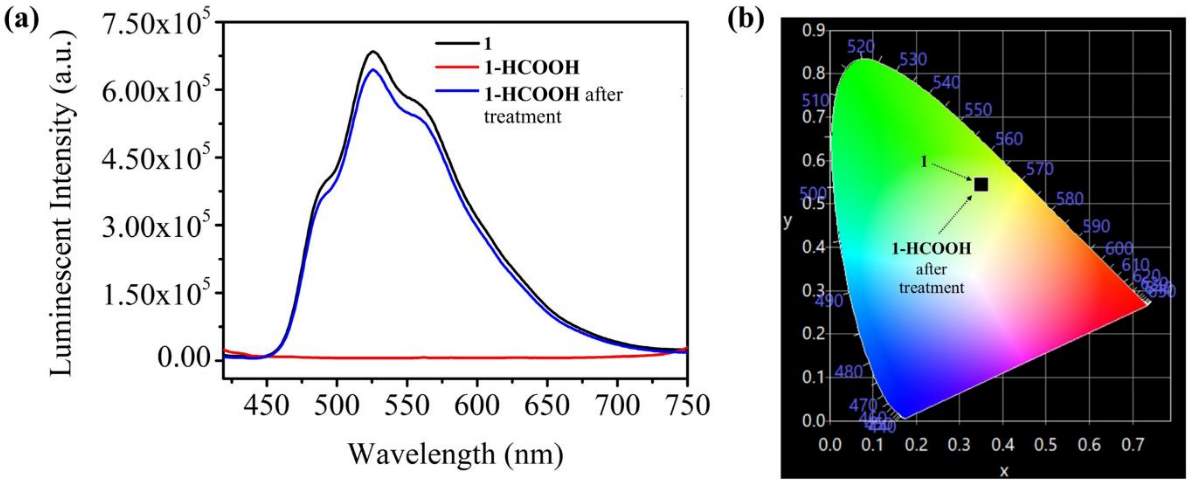

**Fig. S14** The recovery of solid-state PL spectrum (a) and CIE chromaticity coordinate (b) of **1** after treatment of **1-HCOOH** with saturated water vapor ($\lambda_{ex}$ = 389 nm).

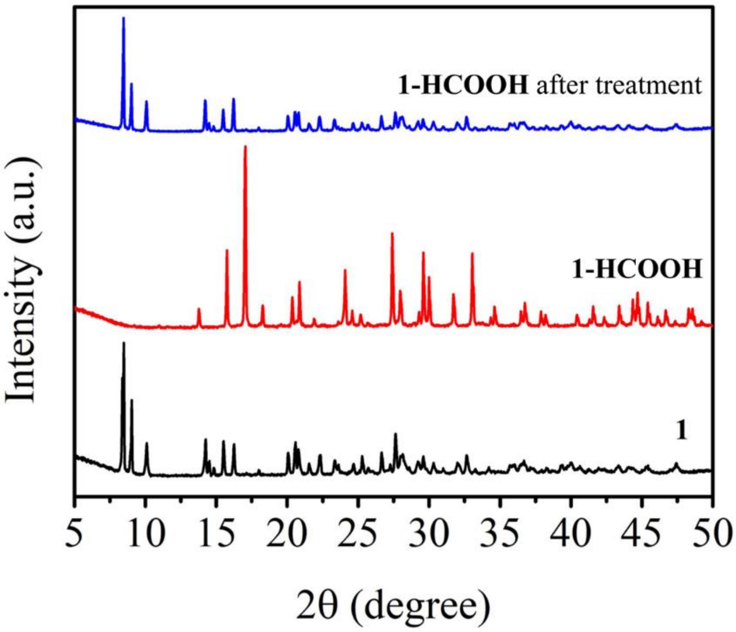

**Fig. S15** The recovered PXRD pattern of **1** after treatment of **1-HCOOH** with saturated water vapor.

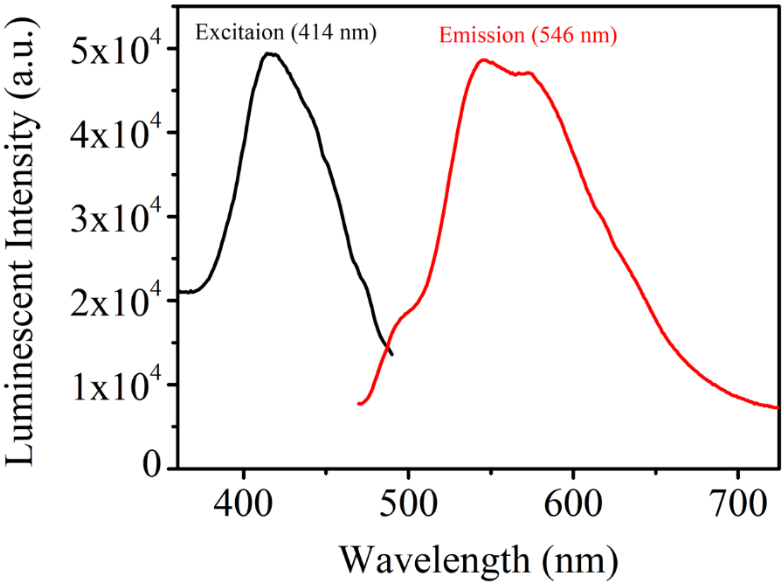

**Fig. S16** Excitation and emission spectra of **1-heat** ($\lambda_{ex}$ = 414 nm and $\lambda_{em}$ = 546 nm) in solid state.

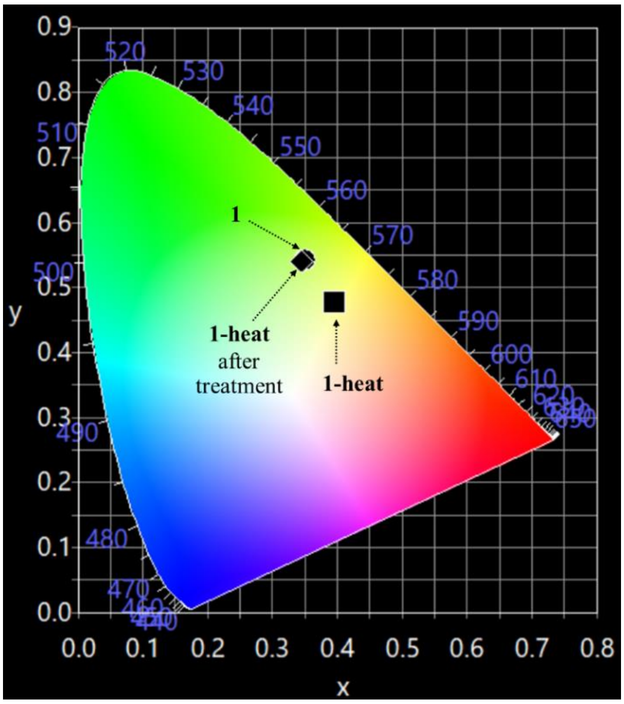

**Fig. S17** CIE chromaticity coordinate of **1**, **1-heat** and **1-heat** after treatment ($\lambda_{ex}$ = 389 nm).

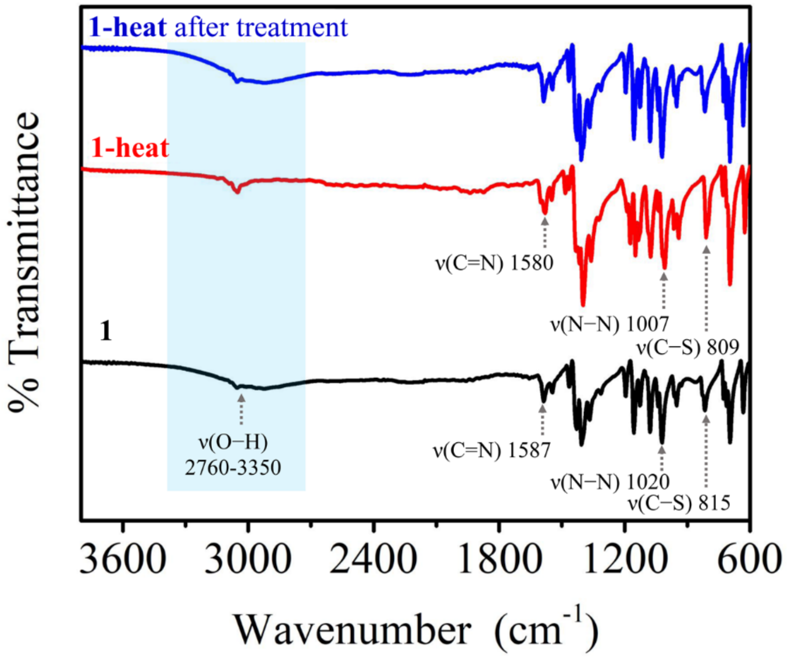

**Fig. S18** FT-IR spectra of **1-heat** and **1-heat** after treatment compared with the original **1**.

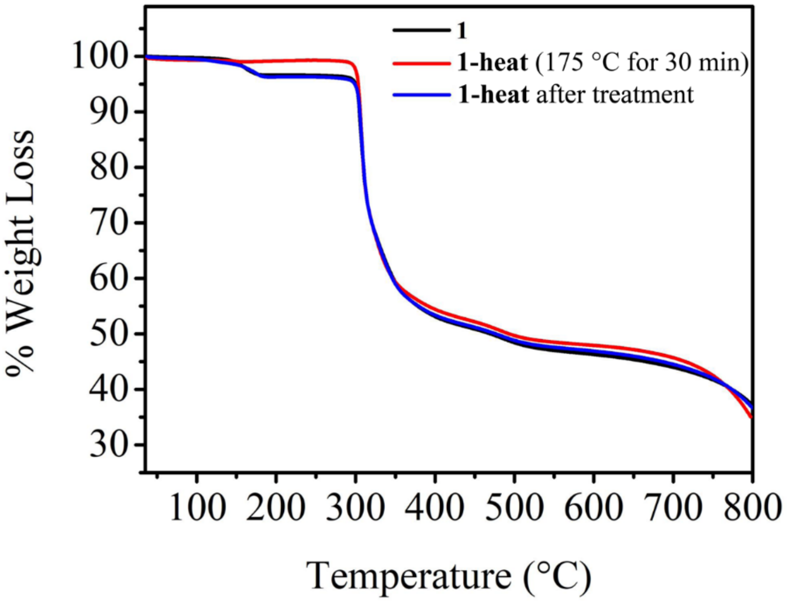

**Fig. S19** TG curves of **1-heat** before and after treatment recorded in $N_2$ atmosphere.

## References

1. *APEX3, SAINT and SADABS*; Bruker AXS Inc.: Madison, WI, USA, 2016.
2. *SAINT 4.0 Software reference manual*; Siemens Analytical X-Ray Systems, Inc.: Madison, WI, 2000.
3. Sheldrick, G. M. *SADABS, Program for empirical absorption correction of area detector data*; University of Göttingen: Göttingen, Germany, 2000.
4. Sheldrick, G. M. A short history of SHELX. *Acta Cryst. A.* **2008**, *64*, 112-122.
5. Sheldrick, G. M. SHELXT - Integrated space-group and crystal-structure determination. *Acta Cryst. A.* 2015, **71**, 3-8.
6. H. Hu, D. Zhao, Y. Gao, X. Qiao, T. Salim, B. Chen, E. E. M. Chia, A. C. Grimsdale and Y. M. Lam, *Chem. Mater.*, 2019, **31**, 2597-2602.
7. X.-S. Wu, Y.-X. Wang, S.-Q. Li, Y. Qian, L. Zhai, X.-Z. Wang and X.-M. Ren, *Dalton Trans.*, 2018, **47**, 14636-14643.
8. X.-K. Tian, J.-R. Zhang, M.-Y. Wen, Z.-H. Liu, J.-h. Guo, C.-Y. Ma, H.-Y. Zhang, X.-G. Yang and L.-F. Ma, *Dalton Trans.*, 2022, **51**, 10055-10060.
9. X.-S. Gao, H.-J. Dai, M.-J. Ding, W.-B. Pei and X.-M. Ren, *Inorg. Chem.*, 2019, **58**, 6772-6780.
10. X.-S. Wu, Y.-R. Tang, J.-L. Liu, L. Wang and X.-M. Ren, *Dalton Trans.*, 2019, **48**, 13841-13849.
11. V. Morad, Y. Shynkarenko, S. Yakunin, A. Brumberg, R. D. Schaller and M. V. Kovalenko, *J. Am. Chem. Soc.*, 2019, **141**, 9764-9768.
12. O. Toma, N. Mercier, M. Allain, F. Meinardi and C. Botta, *Eur. J. Inorg. Chem.*, 2017, **2017**, 844-850.
13. J. Xiang, C. Shen, S.-C. Cheng, F. Yu, W.-K. Chu, H. Feng, S.-M. Yiu, C.-C. Ko and C.-F. Leung, *Dalton Trans.*, 2016, **45**, 16134-16138.
14. L.-X. Wang, J. Xiang, D. Xiang, S.-C. Cheng, C.-F. Leung, C.-C. Ko and J. Xiang, *Inorg. Chem.*, 2022, **61**, 16831-16840.
15. N. N. Golovnev, A. S. Aleksandrovsky, M. A. Gerasimova, F. N. Tomilin, V. A. Mironov, A. V. Demina, Z. Xia and M. S. Molokeev, *ACS Appl. Nano Mater.*, 2021, **4**, 3654-3663.
16. X. Gao, L. Zhao, M. Ding, X. Wang, L. Zhai and X. Ren, *Chin Chem Lett*., 2021, **32**, 2423-2426.
17. X.-S. Wu, R. Zhang and J.-L. Liu, *J. Solid State Chem.*, 2021, **301**, 122298.
18. J.-Y. He, Z.-R. Deng, X. Liu, Y. Qian, Y. Zou and X.-M. Ren, *Dalton Trans.*, 2018, **47**, 9334-9340.
19. X. Liu, L. Zhai, W.-W. Zhang, J.-L. Zuo, Z.-X. Yang and X.-M. Ren, *Dalton Trans.*, 2017, **46**, 7953-7959.
20. J. Sun, D. Zhang, L. Wang, Y. Cao, D. Li, L. Zhang, W. Song, Y. Fan and J. Xu, *CrystEngComm*, 2012, **14**, 3982-3988.

21. J.-X. Ma, Z. Yang, T. Zhou, Q. Guo, J. Yang, T. Yang and Q. Yang, *New J. Chem.*, 2018, **42**, 15413-15419.
22. Q.-Y. Liu and L. Xu, *Eur. J. Inorg. Chem.*, 2006, **2006**, 1620-1628.
23. J. Li, G. Yang, L. Hou, L. Cui, Y. Li, Y.-Y. Wang and Q.-Z. Shi, *Dalton Trans.*, 2013, **42**, 13590-13598.
24. L. Chen, C. Yan, M. Pan, Y.-Z. Fan, L.-Y. Zhang, S.-Y. Yin, Y.-J. Hou, K. Wu, J.-J. Jiang and C.-Y. Su, *New J. Chem.*, 2015, **39**, 5287-5292.
25. J. Lu, S.-H. Wang, Y. Li, W.-F. Wang, C. Sun, P.-X. Li, F.-K. Zheng and G.-C. Guo, *Dalton Trans.*, 2020, **49**, 7309-7314.
26. J. Sun, L. Liu, F. Cheng, M. Hu, W. Qin, R. Huang and G. Wu, *J. Solid State Chem.*, 2019, **277**, 769-772.